IOP PUBLISHING SMART MATERIALS AND STRUCTURES

Smart Mater. Struct. **16** (2007) 1936–1947 doi:10.1088/0964-1726/16/5/051

A single-walled carbon nanotube reinforced 1–3 piezoelectric composite for active control of smart structures

M C Ray and R C Batra

Engineering Science and Mechanics Department, MC 0219, Virginia Polytechnic Institute and State University, Blacksburg, VA 24061, USA

Received 1 December 2006, in final form 12 June 2007
Published 7 September 2007
Online at stacks.iop.org/SMS/16/1936

Abstract
We propose a new 1–3 piezoelectric composite comprised of armchair single-walled carbon nanotubes imbedded in a piezoceramic matrix which we call a NRPEC (nanotube reinforced 1–3 piezoelectric composite). Values of effective piezoelectric and elastic moduli of the NRPEC determined through a micromechanical analysis are found to be significantly higher than those of the 1–3 piezoelectric composite comprised of piezoelectric fibers imbedded in an epoxy matrix. The performance of the NPREC as a constraining layer in an active constrained layer damping (ACLD) treatment of a laminated composite beam has been studied by the finite element method. Both in-plane and out-of-plane actuations by the constraining layer of the ACLD treatment have been considered, and its length has been optimized by implementing a controllability criterion. The computed controllability measure and the frequency response reveal that the proposed constraining layer performs better than the 1–3 piezoelectric/epoxy composite layer.

1. Introduction

The discovery of carbon nanotubes (CNTs) [1] has created enormous interest among researchers to predict their elastic properties. Treacy *et al* [2] experimentally found that the CNTs have axial Young's modulus in the terapascal (TPa) range. Subsequently, many theoretical models have been developed to find elastic properties of CNTs. For example, Lu [3] estimated elastic properties of CNTs and nanoropes using an empirical force constant relation. Ru [4] assumed that a single-walled CNT (SWCNT) can be modeled as a shell and estimated its bending stiffness. Li and Chou [5] computed elastic properties of CNTs by linking structural mechanics and molecular mechanics (MM) approaches. Shen and Li [6] assumed a SWCNT to be transversely isotropic with the axis of transverse isotropy coincident with the tube axis and derived values of the five independent elastic constants by using an energy approach and a MM potential. Whereas investigations [1] through [6] assumed the thickness of a SWCNT, Sears and Batra [7] derived it by simulating simple tensile and torsional deformations of a SWCNT, and assuming its response for infinitesimal deformations to be equivalent to that of a linear elastic, homogeneous and isotropic cylindrical tube of mean diameter equal to that of the SWCNT. They also computed values of Young's modulus and Poisson's ratio, and found that values of the thickness and Young's modulus were essentially independent of the chirality of a SWCNT but depended upon the MM potential used to simulate its deformations. In contrast to Shen and Li's [6] assumption that the axis of transverse isotropy coincided with the geometric axis of a CNT, Batra and Sears [8] have proposed that it be a radial line. Tserpes and Papanikos [9] developed a three-dimensional (3D) finite element (FE) model for predicting Young's modulus and the shear modulus of SWCNTs. Wang *et al* [10] employed a higher order Cauchy–Born rule to estimate mechanical properties of CNTs.

The exceptionally high specific elastic moduli of SWCNTs are being exploited to fabricate CNT-reinforced composites and estimate their mechanical properties. For example, Thostenson *et al* [11] have processed a CNT-reinforced composite, and Thostenson and Chou [12] have estimated its elastic moduli through a micromechanical analysis. Odegard *et al* [13] have modeled the nanotube, the polymer surrounding the tube, and the nanotube/polymer interface as a fiber, and used a micromechanics method to estimate the effective elastic moduli of the CNT-reinforced composite. Linan *et al* [14] have synthesized a CNT-reinforced ceramic composite. Gao and Li [15] have employed a shear lag theory for estimating effective properties of capped CNT-reinforced polymer composites by replacing the tube by an equivalent solid fiber. Wuite and Adali [16] have studied the performance of laminated beams made of CNT-reinforced polymer layers with different angles of orientation of CNTs. For this, they derived elastic properties of aligned, randomly oriented and agglomerated CNT-reinforced polymer composites by employing a micromechanics method while considering the nanotube fibers to be infinitely long, straight and solid. Song and Youn [17] numerically predicted the effective elastic properties of CNT-reinforced polymer based composites. They also demonstrated experimentally how to treat or functionalize the CNT surface to improve the interfacial bonding between the CNT and the matrix and to disperse CNTs uniformly in the epoxy resin. Zhan and Mukherjee [18] fabricated a CNT-reinforced ceramic matrix composite using the spark-plasma-sintering technique. Xia *et al* [19] also fabricated the CNT-reinforced ceramic matrix composite and studied their toughening mechanisms. Since CNTs are being used as reinforcements for developing both polymer and ceramic matrix composites, they may also be used for developing new high performance piezoelectric composites. For example, recently Ramaratnam and Jalili [20] reinforced PVDF (polyvinylidene fluoride) with single-walled and multi-walled CNTs and demonstrated the feasibility of this composite as a sensor material with improved sensing capability. They also speculated that this piezoelectric composite will have enhanced actuating capability over that of PVDF. However, the effective piezoelectric properties of this composite have not been reported.

Piezoelectric materials (PZTs) have been used for distributed sensors and actuators in smart structures [21–43] by exploiting their inherent properties of direct and converse piezoelectric effects. For reliable and efficient control of smart structures, it has been established that when PZTs are used as the constraining layer in an active constrained layer damping (ACLD) treatment, vibrations of smart structures are attenuated much better than when they are directly bonded to the same structures [31–45]. Hence, the performance of two 1–3 piezoelectric composites can be compared by investigating the ACLD of smart structures with constraining layers comprised of these composites and keeping everything else unchanged.

Here we propose a new 1–3 piezoelectric composite, which we call a NRPEC (nanotube reinforced piezoelectric composite), made of a monolithic ceramic PZT reinforced with SWCNTs aligned in the thickness direction, find effective properties of the NRPEC with a micromechanical analysis, and investigate its performance as the material for the constraining layer in the ACLD treatment of a smart beam. It is found that with everything else kept fixed, the NRPEC constraining layer damps out vibrations quickly than a constraining layer comprised of an epoxy matrix reinforced with PZT fibers when both layers have the same weight, length and volume fraction of reinforcing fibers.

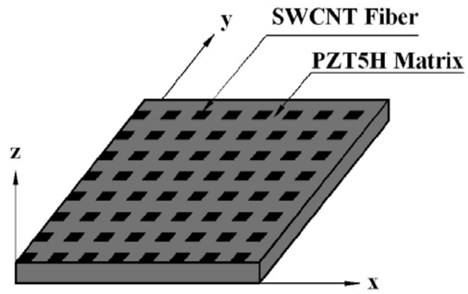

Figure 1. Schematic sketch of a lamina made of SWCNT-reinforced 1–3 piezoelectric composite (NRPEC).

2. Effective properties of the NRPEC

We envisage that in the NRPEC lamina, SWCNTs aligned along the thickness direction, are uniformly distributed; see figure 1. Previous researchers [16, 17] have considered continuum structures equivalent to SWCNTs as either hollow tubular or solid fibers for finding values of material constants. Also, in [15] Young's modulus of the effective solid fiber which is equivalent in mechanical response to a SWCNT is determined from the relation between the elastic moduli of the constituents, their volume fractions and the test value of Young's modulus of the composite. Young's modulus of the effective solid fiber so computed equaled that of a SWCNT found by other techniques. Thus if one replaces the solid circular fiber by one of square cross-section of area equal to that of the circular fiber, it is reasonable to assume that elastic properties of the fiber of square cross-section will be nearly equal to those of the SWCNT. Here such an approximation has been made, and equivalent fiber has been assumed to be transversely isotropic with axis of transverse isotropy coincident with the axis of the fiber. Values of elastic moduli of the fiber are taken to be those derived by Shen and Li [6].

As was done by Smith and Auld [46] for the 1–3 piezoelectric composites in which PZT fibers of square cross-section are imbedded in an epoxy matrix, we use the mechanics of materials approach to derive effective properties of the proposed NRPEC. We note that the PZT/epoxy composite proposed by Smith and Auld [35] is useful for controlling thickness mode oscillations of thin plates. The representative volume element considered for deriving the effective properties is comprised of a SWCNT fiber surrounded by the PZT matrix of the same volume fraction as that in the actual composite. Henceforth we consider only plane strain deformations, and determine effective mechanical properties and piezoelectric coefficients of the NRPEC which quantify induced normal stresses due to the applied electric field E_z across the thickness of the NRPEC lamina to use it as a distributed actuator for laminated composite beams.

Constitutive equations for a SWCNT and a PZT for plane strain deformations in the xz plane can be written as

$$\{\sigma^{\mathrm{n}}\} = [C^{\mathrm{n}}]\{\epsilon^{\mathrm{n}}\} \qquad \text{and} \qquad \{\sigma^{\mathrm{p}}\} = [C^{\mathrm{p}}]\{\epsilon^{\mathrm{p}}\} - \{e^{\mathrm{p}}\}E_z \tag{1}$$

$$\{\sigma^r\} = \begin{Bmatrix} \sigma_x^r \\ \sigma_z^r \\ \sigma_{xz}^r \end{Bmatrix}, \qquad \{\in^r\} = \begin{Bmatrix} \in_x^r \\ \in_z^r \\ \in_{xz}^r \end{Bmatrix},$$

$$[C^r] = \begin{bmatrix} C_{11}^r & C_{13}^r & 0 \\ C_{13}^r & C_{33}^r & 0 \\ 0 & 0 & C_{55}^r \end{bmatrix}, \tag{2}$$

$$\{e^{\mathrm{p}}\} = \begin{Bmatrix} e_{31}^{\mathrm{p}} \\ e_{33}^{\mathrm{p}} \\ 0 \end{Bmatrix}, \qquad r = n \text{ and } p$$

where ($\{\sigma\}$) is the stress, ($\{\in\}$) the strain, $[C]$ the matrix of elastic constants, and $\{e^{\mathrm{p}}\}$ the matrix of piezoelectric coefficients. Superscripts n and p stand for the SWCNT and the PZT, respectively. In equation (2), for the constituent phase r, σ_x^r and σ_z^r represent normal stresses on the x and z planes, respectively; σ_{xz}^r is the transverse shear stress; $\in_x^r$, $\in_z^r$ and $\in_{xz}^r$ are the corresponding infinitesimal strains; C_{ij}^r ($i, j = 1, 2$ and 5) are elastic constants, and e_{31}^{p} and e_{33}^{p} are piezoelectric coefficients of the PZT. It should be noted that same symbols without superscript are used to denote quantities for the NRPEC.

The existence of perfect bonding between the fiber and the matrix is described by the following iso-field or continuity conditions [46, 47]:

$$[\,\sigma_x^{\mathrm{n}} \quad \sigma_{xz}^{\mathrm{n}} \quad \in_z^{\mathrm{n}}\,] = [\,\sigma_x^{\mathrm{p}} \quad \sigma_{xz}^{\mathrm{p}} \quad \in_z^{\mathrm{p}}\,] = [\,\sigma_x \quad \sigma_{xz} \quad \in_z\,]. \tag{3}$$

These express the continuity of surface tractions at the fiber/matrix interface, and the equality of the axial strain in the thickness or the z-direction. Employing the mechanics of materials approach [46], stresses and strains in the homogenized composite are expressed in terms of those of the constituent phases as follows:

$$\begin{gathered} \{\sigma\} = [C_1]\{\in^{\mathrm{n}}\} + [C_2]\{\in^{\mathrm{p}}\} - \{e_1\}E_z, \\ [C_3]\{\in^{\mathrm{n}}\} - [C_4]\{\in^{\mathrm{p}}\} = \{e_2\}E_z \qquad \text{and} \\ \{\in\} = [V_1]\{\in^{\mathrm{n}}\} + [V_2]\{\in^{\mathrm{p}}\} \end{gathered} \tag{4}$$

in which,

$$[C_1] = \begin{bmatrix} 0 & 0 & 0 \\ v_n C_{13}^{\mathrm{n}} & v_n C_{33}^{\mathrm{n}} & 0 \\ 0 & 0 & 0 \end{bmatrix},$$

$$[C_2] = \begin{bmatrix} C_{11}^{\mathrm{p}} & C_{13}^{\mathrm{p}} & 0 \\ v_p C_{13}^{\mathrm{p}} & v_p C_{33}^{\mathrm{p}} & 0 \\ 0 & 0 & C_{55}^{\mathrm{p}} \end{bmatrix},$$

$$\{e_1\} = \begin{Bmatrix} e_{31}^{\mathrm{p}} \\ v_p e_{33}^{\mathrm{p}} \\ 0 \end{Bmatrix}, \qquad [C_3] = \begin{bmatrix} C_{11}^{\mathrm{n}} & C_{13}^{\mathrm{n}} & 0 \\ 0 & 1 & 0 \\ 0 & 0 & C_{55}^{\mathrm{n}} \end{bmatrix}, \tag{5}$$

$$[C_4] = \begin{bmatrix} C_{11}^{\mathrm{p}} & C_{13}^{\mathrm{p}} & 0 \\ 0 & 1 & 0 \\ 0 & 0 & C_{55}^{\mathrm{p}} \end{bmatrix}, \qquad \{e_2\} = \begin{Bmatrix} -e_{31}^{\mathrm{p}} \\ 0 \\ 0 \end{Bmatrix},$$

$$[V_1] = \begin{bmatrix} v_n & 0 & 0 \\ 0 & 1 & 0 \\ 0 & 0 & v_n \end{bmatrix} \qquad \text{and}$$

$$[V_2] = \begin{bmatrix} v_p & 0 & 0 \\ 0 & 0 & 0 \\ 0 & 0 & v_p \end{bmatrix}.$$

Here and below, v_n and v_p represent volume fractions of SWCNTs and the PZT matrix, respectively. Substitution from equation (3) into equation (4) yields the following constitutive relation for the proposed NRPEC:

$$\{\sigma\} = [C]\{\in\} - \{e\}E_z, \tag{6}$$

where $[C]$ and $\{e\}$, the effective elastic and the effective piezoelectric coefficient matrices of the NRPEC, are given by

$$\begin{aligned} &[C] = [C_1][V_3]^{-1} + [C_2][V_4]^{-1}, \\ &[V_3] = [V_1] + [V_2][C_4]^{-1}[C_3], \\ &[V_4] = [V_2] + [V_1][C_3]^{-1}[C_4] \qquad \text{and} \\ &\{e\} = \{e_1\} - [C_1][V_3]^{-1}[V_2][C_4]^{-1}\{e_2\} \\ &\qquad + [C_2][V_4]^{-1}[V_1][C_3]^{-1}\{e_2\}. \end{aligned} \tag{7}$$

Comparing equation (6) with the constitutive relation (1) for a PZT, the effective piezoelectric coefficients e_{31} and e_{33} of the NRPEC can be identified as $e_{31} = e(1)$ and $e_{33} = e(2)$. The effective mass density of the NRPEC is given by the rule of mixtures.

Rather than using the mechanics of materials approach to deduce effective moduli of the NPREC, one could use the principle of equivalent energy, or the Mori–Tanaka method, or the self-consistent method, or Eshelby's approach; e.g. see [47–50].

3. Finite element model of the ACLD of thin composite beams with constraining layer made of NRPEC

In order to investigate the performance of the proposed NRPEC as a candidate material for distributed actuators of smart structures, we develop a FE model of the ACLD of laminated composite thin beams with the constraining layer comprised of the NRPEC. Figure 2 shows a cantilever laminated composite beam composed of N layers and integrated partially with the ACLD treatment on its top surface. The material of each layer is assumed to be homogeneous, orthotropic and linear elastic, and that of the constrained layer of the ACLD treatment homogeneous, isotropic and linear viscoelastic. With appropriate controls, the activated constraining layer should enhance transverse shear deformations of the viscoelastic layer leading to improved energy dissipation of the overall beam. The length, the width and the thickness of the beam are denoted by L, b and h, respectively, while the length of the ACLD treatment by L_a. The thicknesses of the constraining and the constrained layers equal h_p and h_v respectively. The mid-plane of the substrate composite beam is taken as the reference plane for analyzing infinitesimal deformations of the overall system. The origin of the global coordinate system (x, z) is located on this reference plane such that $x = 0$ and L denote end faces of the beam, and a first-order shear deformation theory (FSDT) is used to study its deformations. In figure 2, kinematics of deformation in the x-direction based on the FSDT are illustrated. The variable u_0 represents the translational x-displacement of a point $(x, 0)$ on the reference plane $(z = 0)$; θ_x, ϕ_x and γ_x denote rotations in the xz plane of a normal to the mid-plane of the substrate beam, the viscoelastic layer and the

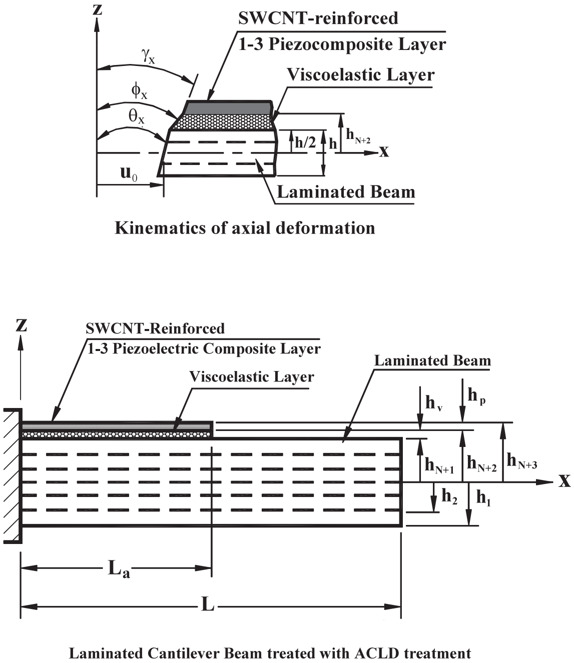

Figure 2. Schematic representation of a laminated composite beam integrated with the ACLD treatment with the NRPEC constraining layer.

piezoelectric composite layer, respectively. Also, as shown in figure 2, the thickness coordinate (z) of the top and the bottom surfaces of the kth layer of the overall beam are denoted by h_{k+1} and h_k, respectively. The axial displacement u of a point in the overall beam is expressed as

$$u(x,z,t) = u_0(x,t) + \left(z - \left\langle z - \frac{h}{2}\right\rangle\right)\theta_x(x,t) + \left(\left\langle z - \frac{h}{2}\right\rangle - \langle z - h_{N+2}\rangle\right)\phi_x(x,t) + \langle z - h_{N+2}\rangle\,\gamma_x(x,t) \tag{8}$$

in which, the bracket $\langle\ \rangle$ defines the appropriate singularity function. Note that equation (8) is for a zigzag beam theory and represents three piecewise continuous expressions for axial displacements in the substrate beam, the viscoelastic layer and the constraining layer. Since, the transverse actuation of the constraining layer of the ACLD treatment can influence flexural vibrations of the beam, the transverse normal strain in the overall beam is also considered. The variation of the transverse displacement (w) across the thickness of the substrate beam, the viscoelastic layer and the constraining layer are assumed to be affine in the thickness coordinate z. Thus similar to the expression (8) for the axial displacement, the transverse displacement of a point is written as

$$w(x,z,t) = w_0(x,t) + \left(z - \left\langle z - \frac{h}{2}\right\rangle\right)\theta_z(x,t) + \left(\left\langle z - \frac{h}{2}\right\rangle - \langle z - h_{N+2}\rangle\right)\phi_z(x,t) + \langle z - h_{N+2}\rangle\,\gamma_z(x,t) \tag{9}$$

in which w_0 equals the transverse displacement of a point on the reference plane; θ_z, ϕ_z and γ_z are the generalized displacements representing gradients with respect to z of the transverse displacement in the substrate beam, the viscoelastic layer and the constraining layer, respectively. We note that displacements u and w within the N layers of the laminated substrate beam are continuous. Thus the continuity of displacements at a point on an interface between two adjoining layers of the beam is satisfied. However, because of possibly different elastic moduli of their materials surface tractions may not be continuous. For a thin beam the discontinuity in surface tractions across an interface does not generally introduce noticeable errors unless magnitudes of their elastic moduli significantly differ. Because of possibly different values of θ_x and ϕ_x in the beam, the viscoelastic layer, and the constraining layer, surface tractions can also be continuous across an interface between two adjoining layers.

For ease of analysis, the generalized displacements are grouped into the following two vectors:

$$\{d_t\} = [\,u_0 \quad w_0\,]^{\mathrm{T}} \qquad \text{and} \qquad \{d_r\} = [\,\theta_x \quad \theta_z \quad \phi_x \quad \phi_z \quad \gamma_x \quad \gamma_z\,]^{\mathrm{T}}. \tag{10}$$

The non-vanishing components of infinitesimal strains at a point in the kth layer are the normal strains $\in_x^k$ and $\in_z^k$ along the x- and the z-directions, respectively, and the transverse shear strain $\in_{xz}^k$. For displacement fields (8) and (9), we have

$$\begin{aligned}
&\{\in_b^k\} = \{\in_{bt}\} + [Z_1]\{\in_{br}\}, \\
&\quad \in_{xz}^k = \in_{st} + [Z_4]\{\in_{sr}\}, \qquad k = 1,2,3,\ldots,N \\
&\{\in_b^k\} = \{\in_{bt}\} + [Z_2]\{\in_{br}\}, \\
&\quad \in_{xz}^k = \in_{st} + [Z_5]\{\in_{sr}\}, \qquad k = N+1 \\
&\{\in_b^k\} = \{\in_{bt}\} + [Z_3]\{\in_{br}\}, \\
&\quad \in_{xz}^k = \in_{st} + [Z_6]\{\in_{sr}\}, \qquad k = N+2
\end{aligned} \tag{11}$$

in which the strain vector $\{\in_b^k\}$, the generalized strains $\{\in_{bt}\}$, $\{\in_{br}\}$, $\in_{st}$, $\{\in_{sr}\}$, and the transformation matrices $[Z_1]$, $[Z_2]$, $[Z_3]$, $[Z_4]$, $[Z_5]$ and $[Z_6]$ are given by

$$\begin{gathered}
\{\in_b^k\} = [\,\in_x^k \quad \in_z^k\,]^{\mathrm{T}}, \qquad \{\in_{bt}\} = \left[\,\tfrac{\partial u_0}{\partial x} \quad 0\,\right]^{\mathrm{T}}, \\
\{\in_{br}\} = \left[\,\tfrac{\partial \theta_x}{\partial x} \quad \tfrac{\partial \phi_x}{\partial x} \quad \tfrac{\partial \gamma_x}{\partial x} \quad \theta_z \quad \phi_z \quad \gamma_z\,\right]^{\mathrm{T}}, \\
\in_{st} = \frac{\partial w_0}{\partial x}, \\
\{\in_{sr}\} = \left[\,\theta_x \quad \phi_x \quad \gamma_x \quad \tfrac{\partial \theta_z}{\partial x} \quad \tfrac{\partial \phi_z}{\partial x} \quad \tfrac{\partial \gamma_z}{\partial x}\,\right]^{\mathrm{T}}, \\
[Z_1] = \begin{bmatrix} z & 0 & 0 & 0 & 0 & 0 \\ 0 & 0 & 0 & 1 & 0 & 0 \end{bmatrix}, \\
[Z_2] = \begin{bmatrix} h/2 & (z-h/2) & 0 & 0 & 0 & 0 \\ 0 & 0 & 0 & 0 & 1 & 0 \end{bmatrix}, \\
[Z_3] = \begin{bmatrix} h/2 & h_v & (z-h_{N+2}) & 0 & 0 & 0 \\ 0 & 0 & 0 & 0 & 0 & 1 \end{bmatrix}, \\
[Z_4] = [\,1 \quad 0 \quad 0 \quad z \quad 0 \quad 0\,], \\
[Z_5] = [\,0 \quad 1 \quad 0 \quad h/2 \quad (z-h/2) \quad 0\,], \\
\text{and} \qquad [Z_6] = [\,0 \quad 0 \quad 1 \quad h/2 \quad h_v \quad (z-h_{N+2})\,].
\end{gathered} \tag{12}$$

The constitutive relation for the material of the kth orthotropic layer of the base beam is given by

$$\{\sigma_b^k\} = [C_b^k]\{\epsilon_b^k\} \quad \text{and} \quad \sigma_{xz}^k = \bar{C}_{55}^k\, \epsilon_{xz}^k; \quad (k = 1, 2, 3, \ldots, N) \tag{13}$$

where

$$\{\sigma_b^k\} = \begin{Bmatrix} \sigma_x^k \\ \sigma_z^k \end{Bmatrix}, \qquad [C_b^k] = \begin{bmatrix} \bar{C}_{11}^k & \bar{C}_{13}^k \\ \bar{C}_{13}^k & \bar{C}_{33}^k \end{bmatrix}$$

and $\bar{C}_{ij}^k$ $(i, j = 1, 3$ and $5)$ are the transformed elastic coefficients with respect to the global coordinate axes. Employing the complex modulus approach for the viscoelastic layer $(k = N + 1)$, its constitutive relation is expressed by equation (13) with $\bar{C}_{ij}^{N+1}$ $(i, j = 1, 3$ and $5)$ being complex numbers [33, 34]. The constitutive relations (6) for the converse and the direct piezoelectric effects of the proposed NRPEC are written as

$$\{\sigma_b^k\} = [C_b^k]\{\epsilon_b^k\} - \{e\}E_z, \qquad \sigma_{xz}^k = \bar{C}_{55}^k\, \epsilon_{xz}^k \quad \text{and} \quad D_z = \{e\}^{\mathrm{T}}\{\epsilon_b^k\} + \varepsilon_{33}E_k; \qquad k = N + 2 \tag{14}$$

in which D_z is the electric displacement along the z-direction, and ε_{33} is the dielectric constant. The piezoelectric coefficient matrix $\{e\}$ and the applied electric field E_z are given by

$$\{e\} = [\, e_{31} \quad e_{33}\,]^{\mathrm{T}} \quad \text{and} \quad E_z = -V/h_p \tag{15}$$

with V being the applied voltage difference across the thickness of the constraining layer.

The principle of virtual work [33] is employed to derive governing equations of the beam/ACLD system, and is expressed as

$$\sum_{k=1}^{N+2} \int_\Omega \left(\{\delta\, \epsilon^k\}^{\mathrm{T}}\{\sigma^k\} + \delta\, \epsilon_{xz}^k\, \sigma_{xz}^k - \delta\{d_t\}^{\mathrm{T}}\rho^k\{\ddot{d}_t\}\right) \mathrm{d}\Omega - \int_\Omega \delta V \varepsilon_{33} V/(h_p)^2\, \mathrm{d}\Omega - \int_A \bar{p}\,\delta w\, \mathrm{d}A = 0 \tag{16}$$

where ρ^k is the mass density of the material of the kth layer, $\bar{p}$ is the externally applied traction on the surface area A, and Ω represents the volume of the kth layer. For the thin beam, the rotary inertia has been neglected in estimating the kinetic energy.

The system is discretized by three-noded isoparametric bar elements. Following equation (10), the generalized displacement vectors associated with the i^{th} $(i = 1, 2, 3)$ node of an element are written as

$$\{d_{ti}\} = [\, u_{0i} \quad w_{0i}\,]^{\mathrm{T}} \quad \text{and} \quad \{d_{ri}\} = [\, \theta_{xi} \quad \theta_{zi} \quad \phi_{xi} \quad \phi_{zi} \quad \gamma_{xi} \quad \gamma_{zi}\,]^{\mathrm{T}}. \tag{17}$$

Thus the generalized displacement vector at a point within an element can be expressed in terms of the nodal generalized displacement vectors $\{d_t^{\mathrm{e}}\}$ and $\{d_r^{\mathrm{e}}\}$ as

$$\{d_t\} = [N_t]\{d_t^{\mathrm{e}}\} \quad \text{and} \quad \{d_r\} = [N_r]\{d_r^{\mathrm{e}}\} \tag{18}$$

where

$$\{d_t^{\mathrm{e}}\} = [\, \{d_{t1}^{\mathrm{e}}\}^{\mathrm{T}} \quad \{d_{t2}^{\mathrm{e}}\}^{\mathrm{T}} \quad \{d_{t3}^{\mathrm{e}}\}^{\mathrm{T}}\,]^{\mathrm{T}},$$

$$[N_t] = [\, N_{t1} \quad N_{t2} \quad N_{t3}\,]^{\mathrm{T}},$$

$$N_i = n_i I_t, \{d_r^{\mathrm{e}}\} = [\, \{d_{r1}^{\mathrm{e}}\}^{\mathrm{T}} \quad \{d_{r2}^{\mathrm{e}}\}^{\mathrm{T}} \quad \{d_{r3}^{\mathrm{e}}\}^{\mathrm{T}}\,]^{\mathrm{T}},$$

$$[N_r] = [\, N_{r1} \quad N_{r2} \quad N_{r3}\,]^{\mathrm{T}} \quad \text{and} \quad N_r = n_r I_r$$

with I_t and I_r being 2×2 and 6×6 identity matrices, respectively, and n_i the shape function in natural coordinates associated with the ith node. Using equations (10), (12), (17) and (18), the generalized strain vectors at a point within an element are expressed as

$$\{\epsilon_{bt}\} = [B_{tb}]\{d_t^{\mathrm{e}}\}, \qquad \{\epsilon_{br}\} = [B_{rb}]\{d_r^{\mathrm{e}}\}, \qquad \epsilon_{st} = [B_{ts}]\{d_t^{\mathrm{e}}\} \quad \text{and} \quad \{\epsilon_{sr}\} = [B_{rs}]\{d_r^{\mathrm{e}}\} \tag{19}$$

in which the nodal strain–displacement matrices $[B_{tb}]$, $[B_{rb}]$, $[B_{ts}]$ and $[B_{rs}]$ are given by

$$[B_{tb}] = [\, B_{tb1} \quad B_{tb2} \quad B_{tb3}\,], \quad [B_{rb}] = [\, B_{rb1} \quad B_{rb2} \quad B_{rb3}\,], \quad [B_{ts}] = [\, B_{ts1} \quad B_{ts2} \quad B_{ts3}\,] \quad \text{and} \quad [B_{rs}] = [\, B_{rs1} \quad B_{rs2} \quad B_{rs3}\,]. \tag{20}$$

Various sub-matrices appearing in equation (20) have the following expressions:

$$B_{tbi} = \begin{bmatrix} \frac{\partial n_i}{\partial x} & 0 \\ 0 & 0 \end{bmatrix}, \qquad B_{tsi} = \begin{bmatrix} 0 & \frac{\partial n_i}{\partial x} \end{bmatrix},$$

$$B_{rbi} = \begin{bmatrix} \frac{\partial n_i}{\partial x} & 0 & 0 & 0 & 0 & 0 \\ 0 & 0 & \frac{\partial n_i}{\partial x} & 0 & 0 & 0 \\ 0 & 0 & 0 & 0 & \frac{\partial n_i}{\partial x} & 0 \\ 0 & n_i & 0 & 0 & 0 & 0 \\ 0 & 0 & 0 & n_i & 0 & 0 \\ 0 & 0 & 0 & 0 & 0 & n_i \end{bmatrix} \tag{21}$$

$$\text{and} \qquad B_{rsi} = \begin{bmatrix} n_i & 0 & 0 & 0 & 0 & 0 \\ 0 & 0 & n_i & 0 & 0 & 0 \\ 0 & 0 & 0 & 0 & n_i & 0 \\ 0 & \frac{\partial n_i}{\partial x} & 0 & 0 & 0 & 0 \\ 0 & 0 & 0 & \frac{\partial n_i}{\partial x} & 0 & 0 \\ 0 & 0 & 0 & 0 & 0 & \frac{\partial n_i}{\partial x} \end{bmatrix}.$$

Substitution from equations (18) and (19) into equation (16) gives the following open loop equations of motion for the coupled beam and the ACLD treatment:

$$[M^{\mathrm{e}}]\{\ddot{d}_t^{\mathrm{e}}\} + [K_{tt}^{\mathrm{e}}]\{d_t^{\mathrm{e}}\} + [K_{tr}^{\mathrm{e}}]\{d_r^{\mathrm{e}}\} = \{F_{tp}^{\mathrm{e}}\}V + \{F^{\mathrm{e}}\} \tag{22}$$

$$[K_{rt}^{\mathrm{e}}]\{d_t^{\mathrm{e}}\} + [K_{rr}^{\mathrm{e}}]\{d_r^{\mathrm{e}}\} = \{F_{rp}^{\mathrm{e}}\}V. \tag{23}$$

The element stiffness matrices $[K_{tt}^{\mathrm{e}}]$, $[K_{tr}^{\mathrm{e}}]$ and $[K_{rr}^{\mathrm{e}}]$, the element electroelastic coupling vectors $\{F_{tp}^{\mathrm{e}}\}$ and $\{F_{rp}^{\mathrm{e}}\}$, the element load vector $\{F^{\mathrm{e}}\}$, and the element mass matrix $[M^{\mathrm{e}}]$ appearing in equations (22) and (23) are given by

$$[K_{tt}^{\mathrm{e}}] = \int_0^{L_{\mathrm{e}}} \left([B_{tb}]^{\mathrm{T}}[D_{tb}][B_{tb}] + [B_{ts}]^{\mathrm{T}}[D_{ts}][B_{ts}]\right) \mathrm{d}x,$$

$$[K_{tr}^{\mathrm{e}}] = \int_0^{L_{\mathrm{e}}} \left([B_{tb}]^{\mathrm{T}}[D_{trb}][B_{rb}] + [B_{ts}]^{\mathrm{T}}[D_{trs}][B_{rs}]\right) \mathrm{d}x,$$

$$\{F_{tp}^{\mathrm{e}}\} = \int_0^{L_{\mathrm{e}}} [B_t]^{\mathrm{T}}\{D_{tp}\}\, \mathrm{d}x,$$

$$[K^{\mathrm{e}}_{rr}] = \int_0^{L_{\mathrm{e}}} \left([B_{rb}]^{\mathrm{T}}[D_{rrb}][B_{rb}] + [B_{rs}]^{\mathrm{T}}[D_{rrs}][B_{rs}]\right) \mathrm{d}x,$$

$$\{F^{\mathrm{e}}_{rp}\} = \int_0^{L_{\mathrm{e}}} [B_r]^{\mathrm{T}}\{D_{rp}\}\,\mathrm{d}x,$$

$$\{F^{\mathrm{e}}\} = \int_0^{L_{\mathrm{e}}} \bar{p}[N_t]^{\mathrm{T}}[0 \quad 1]^{\mathrm{T}}\,\mathrm{d}x \qquad \text{and}$$

$$[M^{\mathrm{e}}] = \sum_{k=1}^{N+2} \rho^k (h_{k+1} - h_k) \int_0^{L_{\mathrm{e}}} [N]^{\mathrm{T}}[N]\,\mathrm{d}x.$$

Elastic stiffness matrices $[D_{tb}]$, $[D_{trb}]$, $[D_{rrb}]$, $[D_{ts}]$, $[D_{trs}]$, $[D_{rrs}]$ and electroelastic constant vectors $\{D_{tp}\}$ and $\{D_{rp}\}$ appearing in equations (22) and (23) are given by

$$[D_{tb}] = \sum_{k=1}^{N+2} \int_{h_k}^{h_{k+1}} [\bar{C}^k_b]\,\mathrm{d}z,$$

$$[D_{trb}] = \sum_{k=1}^{N} \int_{h_k}^{h_{k+1}} [C^k_b][Z_1]\,\mathrm{d}z + \int_{h_{N+1}}^{h_{N+2}} [\bar{C}^{N+1}_b][Z_2]\,\mathrm{d}z + \int_{h_{N+2}}^{h_{N+3}} [\bar{C}^{N+2}_b][Z_3]\,\mathrm{d}z,$$

$$[D_{rrb}] = \sum_{k=1}^{N} \int_{h_k}^{h_{k+1}} [Z_1]^{\mathrm{T}}[\bar{C}^k_b][Z_1]\,\mathrm{d}z + \int_{h_{N+1}}^{h_{N+2}} [Z_2]^{\mathrm{T}}[\bar{C}^{N+1}_b][Z_2]\,\mathrm{d}z + \int_{h_{N+2}}^{h_{N+3}} [Z_3]^{\mathrm{T}}[\bar{C}^{N+2}_b][Z_3]\,\mathrm{d}z,$$

$$[D_{ts}] = \sum_{k=1}^{N+2} \int_{h_k}^{h_{k+1}} \bar{C}^k_{55}\,\mathrm{d}z,$$

$$[D_{trs}] = \sum_{k=1}^{N} \int_{h_k}^{h_{k+1}} C^k_s[Z_4]\,\mathrm{d}z + \int_{h_{N+1}}^{h_{N+2}} \bar{C}^{N+1}_{55}[Z_5]\,\mathrm{d}z + \int_{h_{N+2}}^{h_{N+3}} \bar{C}^{N+2}_{55}[Z_6]\,\mathrm{d}z,$$

$$[D_{rrs}] = \sum_{k=1}^{N} \int_{h_k}^{h_{k+1}} [Z_4]^{\mathrm{T}}\bar{C}^k_{55}[Z_4]\,\mathrm{d}z + \int_{h_{N+1}}^{h_{N+2}} [Z_5]^{\mathrm{T}}\bar{C}^{N+1}_{55}[Z_5]\,\mathrm{d}z + \int_{h_{N+2}}^{h_{N+3}} [Z_6]^{\mathrm{T}}\bar{C}^{N+2}_{55}[Z_6]\,\mathrm{d}z,$$

$$\{D_{tp}\} = \int_{h_{N+2}}^{h_{N+3}} -\{e\}/h_p\,\mathrm{d}z \qquad \text{and}$$

$$\{D_{rp}\} = \int_{h_{N+2}}^{h_{N+3}} -[Z_3]^{\mathrm{T}}\{e\}/h_p\,\mathrm{d}z.$$

Since the matrix of elastic constants of the viscoelastic layer is complex, the stiffness matrices of an element integrated with the ACLD treatment are complex. For an element not integrated with the ACLD treatment, the electroelastic coupling matrices are null vectors and the element stiffness matrices are real. As the stiffness matrices are composed of two parts corresponding to the bending and the transverse shear deformations, we employ a reduced order integration rule (2×2) on terms representing the transverse shear deformation to avoid the shear locking phenomenon generally prevalent in the analysis of a thin beam by the FE method. The element equations are assembled to obtain the following open loop global equations of motion:

$$[M]\{\ddot{X}_t\} + [K_{tt}]\{X_t\} + [K_{tr}]\{X_r\} = \{F_{tp}\}V + \{F\} \tag{24}$$

$$\text{and} \qquad [K_{rt}]\{X_t\} + [K_{rr}]\{X_r\} = \{F_{rp}\}V \tag{25}$$

where $[M]$ is the global mass matrix, $[K_{tt}]$, $[K_{tr}]$ and $[K_{rr}]$ are the global stiffness matrices, $\{F_{tp}\}$, $\{F_{rp}\}$ are the global electroelastic coupling vectors, $\{X_t\}$ and $\{X_r\}$ are the global nodal generalized displacement vectors, and $\{F\}$ is the global nodal force vector. After invoking boundary conditions, the global generalized degrees of freedom $\{X_r\}$ are condensed out to obtain the following equation of motion in terms of the global nodal translational degrees of freedom $\{X_t\}$.

$$[M]\{\ddot{X}_t\} + [K]\{X_t\} = \{F\} + \{F_a\}V \tag{26}$$

where, $[K] = [K_{tt}] - [K_{tr}][K_{rr}]^{-1}[K_{rt}]$ and $\{F_a\} = \{F_{tp}\} - [K_{tr}][K_{rr}]^{-1}\{F_{rp}\}$. Since the stiffness matrix of an element augmented with the ACLD treatment is complex, the global stiffness matrix $[K]$ is complex and the energy dissipation characteristics of the beam are attributed to the imaginary part of this matrix. Thus the global equations of motion (26) also represent the passive (uncontrolled) constrained layer damping of the substrate beam when no voltage difference is applied across the constraining layer.

4. Controllability of the ACLD treatment

In order to investigate the performance of the proposed NRPEC, an optimal control problem is formulated to determine the length of the ACLD treatment that maximizes controllability for different modes of vibrations. Equation (26) is first written in the following standard state space form

$$\{\dot{X}\} = [A]\{X\} + \{B\}V \tag{27}$$

where the system matrix $[A]$, the control input matrix $\{B\}$, and the state vector $\{X\}$ are given by

$$[A] = \begin{bmatrix} O & I \\ -[M]^{-1}[K] & O \end{bmatrix}, \qquad \{B\} = \begin{bmatrix} \tilde{O} \\ [M]^{-1}\{F_a\} \end{bmatrix}$$

$$\text{and} \qquad \{X\} = \begin{bmatrix} \{X_t\} \\ \{\dot{X}_t\} \end{bmatrix}. \tag{28}$$

In matrices $[A]$ and $\{B\}$, O is a null matrix, I an identity matrix, and $\tilde{O}$ a null vector. The controllability criterion proposed by Hamden and Nayfeh [51] has been employed to determine the optimal length of the treatment based on the maximum value of the controllability measure. According to this criterion, the gross measure of controllability of the ith mode due to the control input is assessed by the norm of vector μ defined by

$$\mu = q_i^{\mathrm{T}}\{B\}/\|q_i\| \tag{29}$$

where q_i^{T} is the normalized left eigenvector of $[A]$ for the ith mode such that $q_i^{\mathrm{T}} p_j = \delta_{ij}$ with p_j and δ_{ij} being the right eigenvector of $[A]$ for the jth mode and the Kronecker delta, respectively. For a given substrate beam, the control system matrix $[A]$ and the control input matrix $\{B\}$ vary with the change in the length of the ACLD treatment. Thus the optimal length of the ACLD treatment equals its length that maximizes the value of the controllability measure.

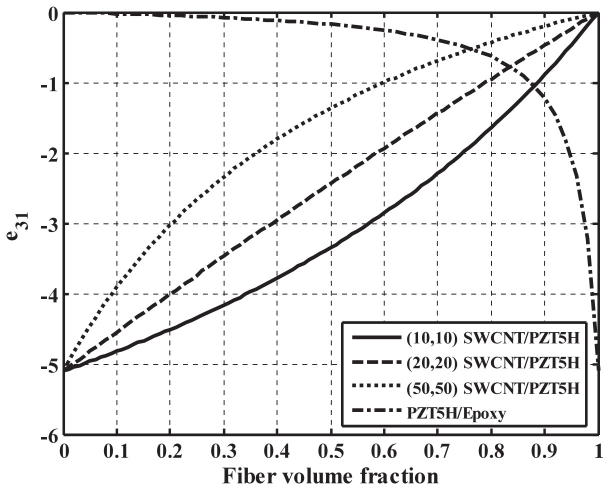

Figure 3. Variation with fiber volume fraction of the effective piezoelectric coefficient, e_{31}, of the NRPEC and the PZT5H/epoxy piezocomposite.

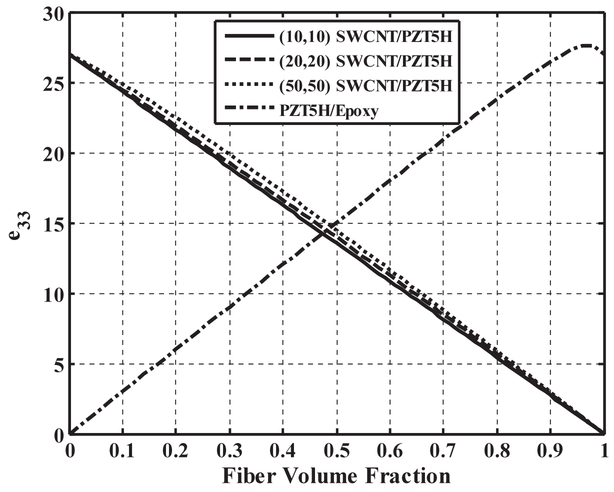

Figure 4. Variation with fiber volume fraction of the effective piezoelectric coefficient, e_{33}, of the NRPEC and thePZT5H/epoxy piezocomposite.

5. Closed loop model

In the active control strategy, we apply a voltage proportional to the translational velocity of the point $(L_a, 0)$ of the free end of the ACLD treatment of the constraining layer. Thus

$$V = -k_d \dot{w}(L_a, 0) = -k_d[U]\{\dot{X}\} \tag{30}$$

where k_d is the gain factor, and $[U]$ a row vector relating the velocity of the point $(L_a, 0)$ to the time derivatives of the global nodal generalized translational displacements. By substituting for V from equation (30) into (26), we obtain the following equation of motion governing the closed loop behavior of the overall beam/ACLD system

$$[M]\{\ddot{X}\} + [C_d]\{\dot{X}\} + [K]\{X\} = \{F\} \tag{31}$$

where $[C_d] = k_d\{F_a\}[U]$ is the active damping matrix.

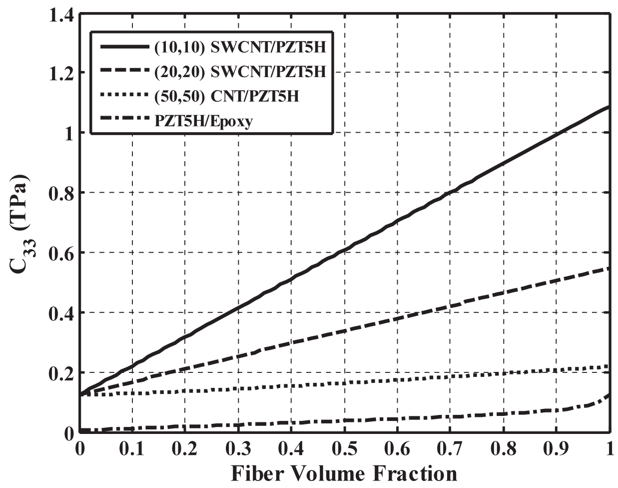

Figure 5. Variation with fiber volume fraction of the effective elastic coefficient, C_{33}, of the NRPEC and the PZT5H/epoxy piezocomposite.

6. Results and discussion

In the following sample problems we consider armchair SWCNTs and the PZT5H as materials for fibers and the matrix, respectively, and values of their material parameters are listed in table 1. Both the SWCNTs and the PZT5H are taken to be transversely isotropic with the axis of transverse isotropy along the z-axis that is along the thickness of the NRPEC lamina. Figures 3 and 4 illustrate, respectively, variation with the fiber volume fraction of the effective piezoelectric coefficients e_{31} and e_{33} of the proposed NRPEC. The effective values of e_{31} and e_{33} for the 1–3 PZT5H/epoxy composite analyzed by Smith and Auld [46] are also included in these figures. It is clear that, at low fiber volume fractions, magnitudes of the effective piezoelectric coefficients of the proposed NRPEC are significantly higher than those of the PZT5H/epoxy. This is because elastic moduli of both the fiber and the matrix of the NRPEC are higher than those of the PZT5H/epoxy composite. The effective elastic constants of the proposed NRPEC are also higher than those of the PZT5H/epoxy composite as can be seen from figure 5 where only C_{33} is plotted. Shen and Li's [6] data indicates that magnitudes of elastic constants of SWCNTs decrease with an increase in their diameter. Thus values of the effective piezoelectric coefficient e_{31} and the elastic constant C_{33} of the NRPEC decrease with an increase in the diameter of the SWCNT (figures 3 and 5). It can be concluded from results plotted in figure 4 that the effective value of e_{33} of the NRPEC is independent of the diameter of the SWCNT.

Even though results in figures 3–5 are plotted for large values of volume fractions of the SWCNT, in practice a uniform distribution of CNTs is obtained only for a rather small volume fraction of SWCNTs. The goal here is to show that the performance of the NRPEC as a material for actuators is superior to that of conventional piezocomposites. We neither address fabricability nor cost of the NRPEC.

To demonstrate the performance of the NRPEC as a material for distributed actuators of smart structures, the ACLD of a cantilever laminated composite beam with the constraining layer made of the NRPEC is investigated. Values of elastic

Table 1. Material properties of the constituent phases of the NRPEC.

Material	Source	C_{11} (GPa)	C_{12} (GPa)	C_{13} (GPa)	C_{33} (GPa)	C_{44} (GPa)	e_{31}^{p} (C m^{-2})	e_{33}^{p} (C m^{-2})
SWCNT (10, 10)	[6]	288	254	87.8	1088	442	—	—
SWCNT (20, 20)	[6]	138	134	43.5	545	227	—	—
SWCNT (50, 50)	[6]	55.1	54.9	17.5	218	92	—	—
PZT5H	[35]	151	98	96	124	23	−5.1	27
Spurr	[35]	5.3	3.1	3.1	5.3	0.64	—	—

Table 2. Non-dimensional natural frequencies $\varpi = \omega L^2\sqrt{\rho/(E_{\mathrm{L}}h^2)}$ of the substrate beam with negligible thickness of the ACLD treatment.

Beams	Source	1st mode	2nd mode	3rd mode
$(0°/90°/90°/0°)$	Present FEM	0.9238	4.8872	11.4385
	Ref. [52]	0.9241	4.8925	11.4400
$(45°/-45°/45°/-45°)$	Present FEM	0.2947	1.8147	4.9087
	Ref. [53]	0.2962	1.8156	4.9163

moduli of an orthotropic layer of the graphite/epoxy substrate beam, in the material principal directions, are

$$E_{\mathrm{L}} = 172 \text{ GPa}, \qquad E_{\mathrm{L}}/E_{\mathrm{T}} = 25,$$

$$G_{\mathrm{LT}} = 0.5E_{\mathrm{T}}, \qquad \upsilon_{\mathrm{LT}} = 0.25$$

where E_{L} and E_{T} are Young's moduli in the longitudinal and the transverse directions respectively, and G_{LT} and υ_{LT} the shear modulus and Poisson's ratio in the xz plane. Unless otherwise mentioned, the orthotropic layers of the substrate beam are of equal thickness with the length and the thickness of the beam set equal to 0.5 m and 5 mm, respectively. The complex shear modulus, Poisson's ratio and the mass density of the constrained viscoelastic layer are taken [34] as $20(1+i)$ MPa, 0.3 and 1140 kg m^{-3}, respectively. Also, since the performance of the proposed NRPEC will be compared with that of the 1–3 PZT5H/epoxy composite with 40% PZT5H fibers by volume, the thickness of the constraining layer made of the NRPEC is chosen so that for a particular length the two constraining layers have the same weight. Thus the thickness of the constraining layer of the NRPEC is given by

$$h_p\Big|_{\mathrm{SWCNT/PZT5H}} = \left(\rho^{N+2}_{\mathrm{SWCNT/PZT5H}}/\rho^{N+2}_{\mathrm{PZT5H/Epoxy}}\right)h_p\Big|_{\mathrm{PZT5H/Epoxy}}. \tag{32}$$

In order to validate the **FE** model developed here, a specimen is considered in which thickness (0.001 μm) of the ACLD treatment is negligible as compared to the 0.005 m of the substrate beam. Presently computed natural frequencies are compared in table 2 with those obtained by other investigators [52, 53]. It is clear that the two sets of values agree well with each other.

To determine the optimum length of the ACLD treatment, we have displayed in figure 6 the variation with the length of the ACLD treatment of the controllability measure, μ, defined by equation (29) for the proposed NRPEC and the PZT5H/epoxy constraining layers for controlling the first mode of vibration of a symmetric cantilever cross-ply $(0°/90°/0°)$ beam. It is clear that the maximum controllability is achieved when the length of the ACLD treatment equals 70% of the length of the substrate beam, and the maximum controllability for the NRPEC is significantly higher than that of the PZT5H/epoxy composite. This is attributed to the fact that values of effective piezoelectric coefficients (e_{31}, e_{33}) of the proposed NRPEC are larger than those of the PZT5H/epoxy composite. We note the controllability of the constraining layer decreases with an increase in volume fraction of the SWCNTs. For controlling the second and the third modes of vibration, the maximum controllability is achieved when the length of the treatment equals 90% and 100% of the beam length (cf figures 7 and 8) and for each case the controllability of the NRPEC constraining layer is larger than that of the PZT5H/epoxy composite. Similar results are obtained for antisymmetric angle-ply laminated substrate beams. However, for the sake of brevity, the variation with the length of the ACLD treatment of the controllability measure for the first three modes of vibration of the $(-45°/45°/-45°/45°)$ beam are displayed in figure 9. Values of L_a/L for the maximum controllability of the first, the second, and the third modes of vibration equal 0.65, 0.9 and 1.0, respectively.

In order to investigate the frequency response for the ACLD of a cantilever laminated beam using the proposed NRPEC with 20% fiber volume fraction of SWCNTs, the length of the ACLD treatment is set equal to 65% of the length of the substrate beam. For 1 mm thickness of PZT5H/epoxy layer, the thickness of the NRPEC constraining layer determined from equation (32) equals 0.582 mm. To compute the frequency response functions, the beam is harmonically excited by a force of 2 N at its free end. For three values of the gain factor, figure 10 illustrates frequency response functions for the transverse displacement, w, of the free end $(L, 0)$ of a symmetric cross-ply $(0°/90°/0°)$ beam. Both uncontrolled (passive or gain factor equal to zero) and controlled responses displayed in this figure clearly reveal that the NRPEC constraining layer significantly attenuates the amplitude of vibrations and enhances the damping characteristics of the beam over those of the passively damped (uncontrolled) beam. In figures 11 and 12 we have compared the performance of the NRPEC with that of the PZT5H/epoxy composite. It is known that the ACLD of smart

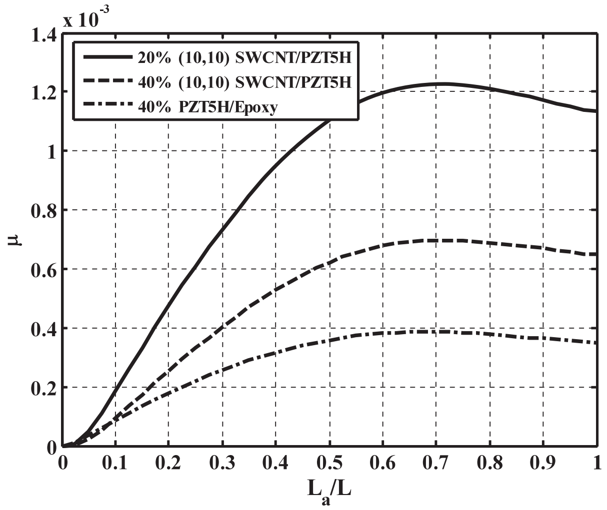

Figure 6. Variation of controllability of the ACLD treatment with length for controlling the first mode of vibration of a cantilever cross-ply (0°/90°/0°) beam with the constraining layer comprised of the NRPEC and the PZT5H/epoxy piezocomposite.

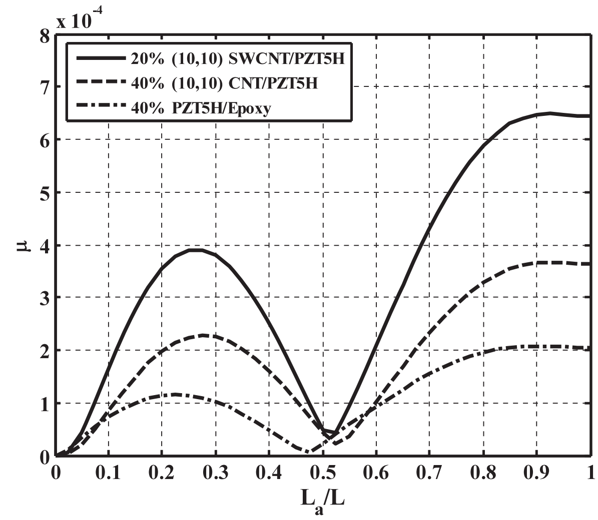

Figure 7. Variation of controllability of the ACLD treatment with length for controlling the second mode of vibration of a cantilever cross-ply (0°/90°/0°) beam with the constraining layer comprised of the NRPEC and the PZT5H/epoxy piezocomposite.

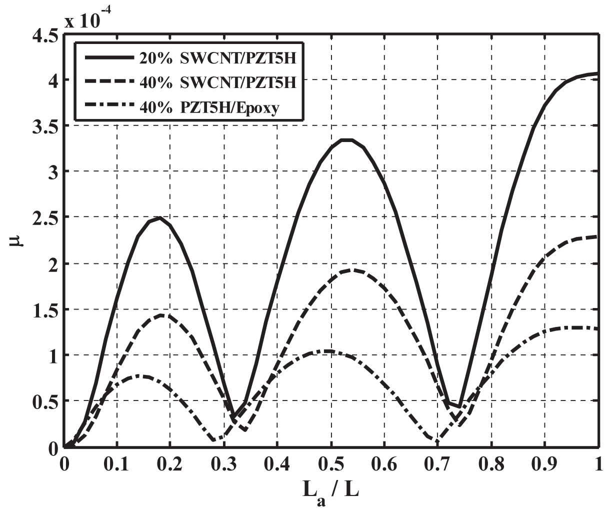

Figure 8. Variation of controllability of the ACLD treatment with length for controlling the third mode of vibration of a cantilever cross-ply (0°/90°/0°) beam with the constraining layer comprised of the NRPEC and the PZT5H/epoxy piezocomposite.

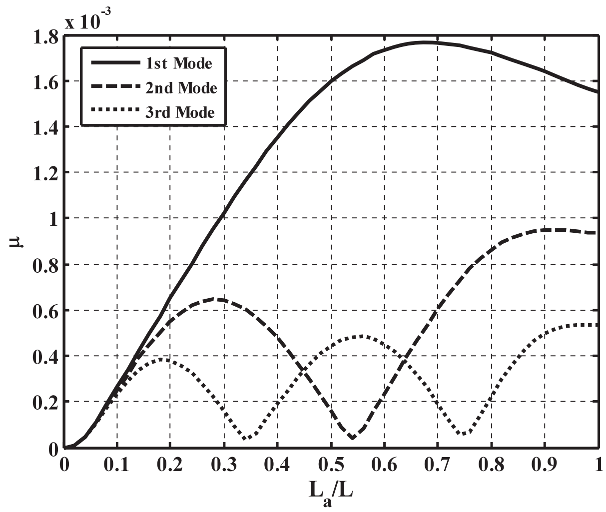

Figure 9. Variation of controllability of the ACLD treatment with length for controlling the first three modes of vibration of a cantilever cross-ply (45°/45°/–45°/45°) beam with the constraining layer comprised of the NRPEC and the PZT5H/epoxy piezocomposite.

structures is attributed to the transverse shear deformation of the constrained viscoelastic layer. The increase in the transverse shear deformation of the constrained viscoelastic layer caused by the addition of the constraining layer depends on the magnitudes of the piezoelectric coefficients of the constraining layer. Since values of the effective piezoelectric coefficients (e_{31}, e_{33}) of the proposed NRPEC are higher than those of the PZT5H/epoxy composite, therefore the NRPEC enhances the attenuation of vibrations of the beam. Furthermore, the control voltage required by the NRPEC constraining layer is less than that for the PZT5H/epoxy composite (cf figure 12). Whereas Batra and Geng [35] computed the energy required to annul vibrations of a plate, we have not done so.

As illustrated in figure 13, contributions from the in-plane and the transverse actuations of the proposed NRPEC constraining layer for improving damping characteristics of the beam can be ascertained by fixing the gain factor to say 2000 and setting either e_{33} or e_{31} equal to zero. For $e_{31} = 0$ and $e_{33} \neq 0$, an applied electric field to the NRPEC constraining layer in the z-direction induces transverse strains in it. However, for $e_{33} = 0$ and $e_{31} \neq 0$, the same electric field causes in-plane deformations of the NRPEC constraining layer. When both e_{31} and e_{33} are nonzero, the active damping of the beam is attributed to both the in-plane and the transverse deformations of the constraining layer. It is evident from results presented in figure 13 that both the in-plane and the transverse actuations of the NRPEC constraining layer occur in unison and hence improve damping characteristics of the

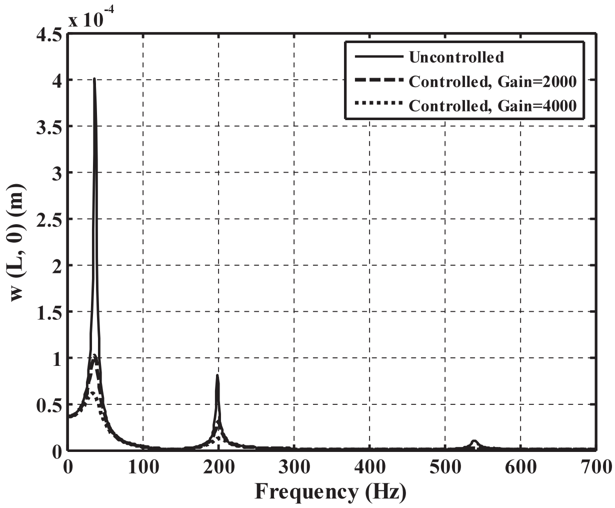

Figure 10. Variation with frequency of excitation of the transverse displacement of the free end of a cross-ply (0°/90°/0°) cantilever beam with the ACLD treatment.

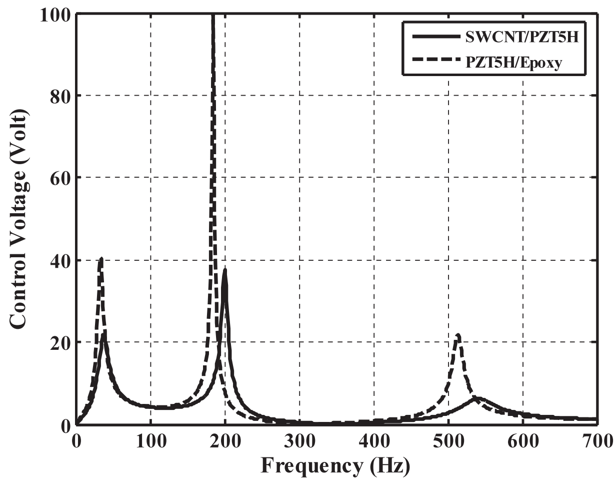

Figure 12. Variation with frequency of the control voltage for the ACLD of the cantilever cross-ply (0°/90°/0°) beam obtained by using the NRPEC and the PZT5H/epoxy piezocomposite.

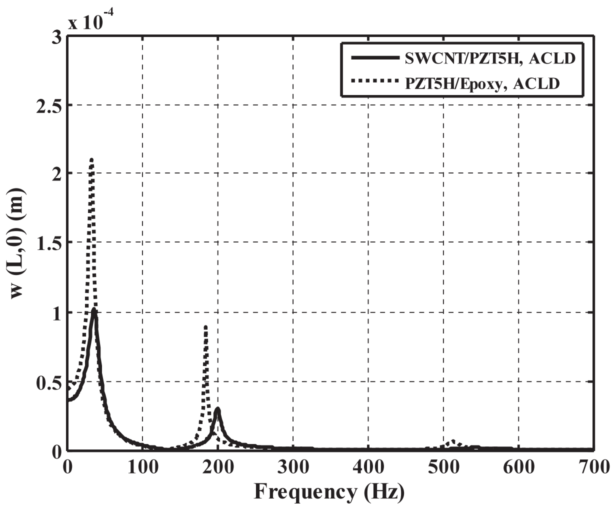

Figure 11. Comparison of the controlled responses for the ACLD of the cantilever cross-ply (0°/90°/0°) beam obtained by using the NRPEC and PZT5H/epoxy piezocomposite.

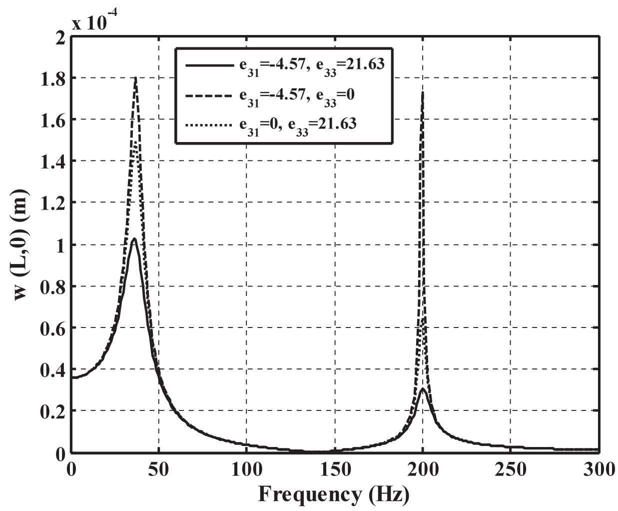

Figure 13. For three combinations of values of e_{31} and e_{33}, variation with frequency of the tip deflection of the cantilever cross-ply (0°/90°/0°) beam integrated with the ACLD treatment.

beam. However, the contribution of the transverse actuation is larger than that of the in-plane actuation. Frequency response functions for the ACLD of antisymmetric angle-ply beams are found to be similar to those illustrated in figure 10 for a cross-ply beam, and for the sake of brevity are omitted.

Results presented above are for the NRPEC containing 20% volume fraction of uniformly distributed SWCNTs. However, in practice, it has not been feasible to achieve this thus far. With improvements in manufacturing technologies and enhanced functionalization of SWCNTs, one may attain this in future. When the SWCNTs are not aligned in the thickness direction, then the deduction of effective moduli by the mechanics of materials approach will give very approximate values of the effective moduli and a more realistic approach is to use a method adopted in [39–41]. We note that Vidoli and Batra [54] have used a higher order shear and normal deformation theory to analyze electromechanical deformations of a PZT beam with the axis of transverse isotropy not necessarily aligned along the thickness of the beam.

We have assumed linear constitutive relations for the NRPEC, the viscoelastic layer, and the material of the beam. Batra and Liang [41] and Batra and Geng [35] have incorporated material and geometric nonlinearities in formulating three-dimensional problems for smart structures, and analyzing the active control of their vibrations by the finite element method.

7. Conclusions

We have proposed a new 1–3 piezoelectric composite (NRPEC) comprised of single-walled carbon nanotube (SWCNT) reinforcements and a monolithic piezoceramic (PZT5H) matrix. A micromechanical analysis has been carried out to predict effective piezoelectric and elastic moduli of the NRPEC. It is found that at low volume fractions of SWCNTs, the effective piezoelectric and the effective elastic moduli of the NRPEC are significantly higher than those of the 1–3 PZT5H/epoxy composite. To investigate the performance of the NRPEC as an actuator material for smart structures, the active constrained layer damping (ACLD) of a cantilever laminated composite beam has been studied. Both in-plane and out-of-plane actuations of the constraining layer have been considered. We have developed a finite element model of a beam with the ACLD treatment incorporating transverse deformations of the substrate beam, the constrained viscoelastic layer, and the constraining layer to describe dynamics of the system. A controllability criterion has been implemented to determine the optimal length of the ACLD treatment for annulling a desired mode of vibration of the system. It is found that the controllability of vibration of the ACLD treatment with the NRPEC constraining layer is significantly larger than that of the PZT5H/epoxy composite of the same mass. The frequency responses for the ACLD of symmetric cross-ply and antisymmetric angle-ply composite beams have revealed the improved attenuating capability of the NRPEC constraining layer over that of the PZT5H/epoxy layer. This is due to both in-plane and out-of-plane actuations induced by the NRPEC constraining layer. Thus the distributed NRPEC actuators can be used to control vibrations of lightweight structures.

Acknowledgments

This work was partially supported by ONR grants N00014-1-98-0300 and N00014-1-06-0567 to Virginia Polytechnic Institute and State University (VPI&SU) with Dr Y D S Rajapakse as the program manager. Views expressed herein are those of the authors and do not express those of the funding agency nor of VPI&SU.

References

[1] Iijima S 1991 Helical microtubes of graphitic carbon *Nature* **354** 56–8
[2] Treacy M M J, Ebbessen T W and Gibson J M 1996 Exceptionally high Young's modulus observed for individual carbon nanotubes *Nature* **381** 678–80
[3] Lu J P 1997 Elastic properties of carbon nanotubes and nanoropes *Phys. Rev. Lett.* **79** 1297–300
[4] Ru C Q 2000 Effective bending stiffness of carbon nanotubes *Phys. Rev.* B **62** 9973–6
[5] Li C and Chou T W 2003 A structural mechanics approach for the analysis of carbon nanotubes *Int. J. Solids Struct.* **40** 2487–99
[6] Shen L and Li J 2004 Transversely isotropic elastic properties of single-walled carbon nanotubes *Phys. Rev.* B **69** 045414
[7] Sears A and Batra R C 2004 Macroscopic properties of carbon nanotubes from molecular mechanics simulations *Phys. Rev.* B **69** 235406
[8] Batra R C and Sears A 2007 Uniform radial expansion/contraction of carbon nanotubes and their transverse elastic moduli *Modelling Simul. Mater. Sci. Eng.* submitted
[9] Tserpes K I and Papanikos P 2005 Finite element modeling of single-walled carbon nanotube *Composites* B **36** 468–77
[10] Wang J B, Guo X, Zhang H W, Wang L and Liao J B 2006 Energy and mechanical properties of single-walled carbon nanotubes predicted using the higher order Cauchy Born rule *Phys. Rev.* B **73** 115428
[11] Thostenson E T, Li W Z, Wang D Z, Ren Z F and Chou T W 2002 Carbon nanotube/carbon fiber hybrid multiscale composites *J. Appl. Phys.* **91** 6034–41
[12] Thostenson E T and Chou T W 2003 On the elastic properties of carbon nanotube based composites: modeling and characterization *J. Phys. D: Appl. Phys.* **36** 573–82
[13] Odegard G M, Gates T S, Wise K E, Park C and Siochi E J 2003 Constitutive modeling of nanotube-reinforced polymer composites *Compos. Sci. Technol.* **63** 1671–87
[14] Linan A *et al* 2004 Carbon nanotube reinforced polymer-derived ceramic composites *Adv. Mater.* **16** 2036–40
[15] Gao X L and Li K 2005 A shear-lag model for carbon nanotube reinforced polymer composites *Int. J. Solids Struct.* **42** 1649–67
[16] Wuite J and Adali S 2005 Deflection and stress behavior of nanocomposite reinforced beams using a multiscale analysis *Compos. Struct.* **71** 388–96
[17] Song Y S and Youn J R 2006 Modeling of effective elastic properties for polymer based carbon nanotube composites *Polymer* **47** 1741–8
[18] Zhan G-D and Mukherjee A K 2004 Carbon nanotube reinforced alumina-based ceramics with novel mechanical, electrical, and thermal properties *Int. J. Appl. Ceram. Technol.* **1** 161–71
[19] Xia Z, Riester L, Curtin W A, Li H, Sheldon B W, Liang J, Chang B and Xu J M 2004 Direct observation of toughening mechanisms in carbon nanotube ceramic matrix composites *Acta Mater.* **52** 931–44
[20] Ramaratnam A and Jalili N 2006 Reinforcement of piezoelectric polymer with carbon nanotubes: pathway to next generation sensors *J. Intell. Mater. Syst. Struct.* **17** 199–208
[21] Bailey T and Hubbard J E 1985 Distributed piezoelectric polymer active vibration control of a cantilever beam *J. Guid. Control Dyn.* **8** 605–11
[22] Crawley E F and Luis J D 1987 Use of piezoelectric actuators as elements of intelligent structures *AIAA J.* **25** 1373–85
[23] Baz A and Poh S 1988 Performance of an active control system with piezoelectric actuators *J. Sound Vib.* **126** 327–43
[24] Lee C K, Chiang W W and Sullivan O 1991 Piezoelectric modal sensor/actuator pairs for critical active damping vibration control *J. Acoust. Soc. Am.* **90** 374–84
[25] Hanagud S, Obal M W and Calise A J 1992 Optimal vibration control by the use of piezoceramic sensors and actuators *J. Guid. Control Dyn.* **15** 1199–206
[26] Gu Y, Clark R L and Fuller C R 1994 Experiments on active control of plate vibration using piezoelectric actuators and polyvinylidyne fluoride (PVDF) modal sensors *ASME J. Vib. Acoust.* **116** 303–8
[27] Baz A and Poh S 1996 Optimal vibration control with modal positive position feedback *Opt. Control Appl. Methods* **17** 141–9
[28] Agarwal B N and Treanor K E 1999 Shape control of a beam using piezoelectric actuators *Smart Mater. Struct.* **8** 729–40
[29] Sun D C and Tong L 2001 Vibration Control of Plates using discretely distributed piezoelectric quasi-modal actuators/sensors *AIAA J.* **39** 1766–72
[30] Ray M C 2003 Optimal control of laminated shells with piezoelectric sensor and actuator layers *AIAA J.* **41** 1151–7
[31] Azvine B, Tomlinson G R and Wynne R J 1995 Use of active constrained layer damping for controlling resonant *Smart Mater. Struct.* **4** 1–6
[32] Ray M C and Baz A 1997 Optimization of energy dissipation of active constrained layer damping treatments of plates *J. Sound Vib.* **208** 391–406
[33] Jeung Y S and Shen I Y 2001 Development of isoparametric, degenerate constrained layer element for plate and shell structures *AIAA J.* **39** 1997–2005
[34] Chantalakhana C and Stanway R 2001 Active constrained layer damping of clamped–clamped plate vibrations *J. Sound Vib.* **241** 755–77

[35] Batra R C and Geng T S 2002 Comparison of active constrained layer damping by using extension and shear mode actuators *J. Intell. Mater. Syst. Struct.* **13** 249–367
[36] Ray M C and Reddy J N 2004 Optimal control of thin circular cylindrical shells using active constrained layer damping treatment *Smart Mater. Struct.* **13** 64–72
[37] Ghosh K and Batra R C 1995 Shape control of plates using piezoceramic elements *AIAA J.* **33** 1354–7
[38] Batra R C and Ghosh K 1995 Deflection control during dynamic deformations of a rectangular plate using piezoceramic elements *AIAA J.* **33** 1547–8
[39] Batra R C, Liang X Q and Yang J S 1996 Shape control of vibrating simply supported plates *AIAA J.* **34** 116–22
[40] Batra R C and Liang X Q 1997 The vibration of a rectangular laminated elastic plate with embedded piezoelectric sensors and actuators *Comput. Struct.* **63** 203–16
[41] Batra R C and Liang X Q 1997 Finite dynamic deformations of smart structures *Comput. Mech.* **20** 427–38
[42] Vel S S and Batra R C 2000 Cylindrical bending of laminated plates with distributed and segmented piezoelectric actuator/sensors *AIAA J.* **38** 857–67
[43] Vel S S and Batra R C 2001 Analysis of piezoelectric bimorphs and plates with segmented actuators *J. Thin-Walled Struct.* **39** 23–44
[44] Vel S S and Batra R C 2001 Exact solution for the cylindrical bending of laminated plates with embedded shear actuators *Smart Mater. Struct.* **10** 240–51
[45] Vel S S and Batra R C 2001 Exact solution for rectangular sandwich plates with embedded piezoelectric shear actuators *AIAA J.* **39** 1363–73
[46] Smith W A and Auld B A 1991 Modeling 1–3 composite piezoelectrics: thickness mode oscillations *IEEE Trans. Ultrason. Ferroelectr. Freq. Control* **31** 40–7
[47] Benveniste Y and Dvorak G J 1992 Uniform fields and universal relations in piezoelectric composites *J. Mech. Phys. Solids* **40** 1295–312
[48] Jiang B and Batra R C 2001 Micromechanical modeling of a composite containing piezoelectric and shape memory alloy inclusions *J. Intell. Mater. Syst. Struct.* **12** 165–82
[49] Jiang B and Batra R C 2002 Effective properties of a piezocomposite containing shape memory alloy and inert inclusions *Contin. Mech. Thermodyn.* **14** 87–111
[50] Jiang B and Batra R C 2001 Effective electroelastic properties of a piezocomposite with viscoelastic and dielectric relaxing matrix *J. Intell. Mater. Syst. Struct.* **12** 847–66
[51] Hamden A M A and Nayfeh A H 1989 Measure of modal controllability and observability for first and second order linear systems *J. Guid. Control Dyn.* **12** 421–8
[52] Chandrashekhara K, Krishnamurthy K and Roy S 1990 Free vibration of composite beams including rotary inertia and shear deformation *Compos. Struct.* **14** 269–79
[53] Chandrashekhara K and Bangera K M 1992 Free vibration of composite beams using a refined shear flexible beam element *Comput. Struct.* **43** 719–27
[54] Vidoli S and Batra R C 2000 Derivation of plate and rod equations for a piezoelectric body from a mixed three-dimensional variational principle *J. Elast.* **59** 23–50